OH binding energy as a universal descriptor of the potential of zero charge on transition metal surfaces

Sara Kelly,[†,‡] Hendrik H. Heenen,[¶,‡] Nitish Govindarajan,[¶,‡] Karen Chan,[*,¶] and Jens K. Nørskov[*,¶]

†*Department of Chemical Engineering, Stanford University, Stanford, California 94305-6104, United States*

‡*These authors contributed equally*

¶*Catalysis Theory Center, Department of Physics, Technical University of Denmark, 2800 Kgs. Lyngby, Denmark*

E-mail: kchan@fysik.dtu.dk; jkno@dtu.dk

Abstract

The potential of zero charge (U_{PZC}) is an important quantity of metal-water interfaces that are central in many electrochemical applications. In this work, we use *ab initio* molecular dynamics (AIMD) simulations to study a large number of (111), (100), (0001) and (211) and overlayers of transition metal-water interfaces in order to identify simple descriptors to predict their U_{PZC}. We find a good correlation between water coverage and the work function reduction $\Delta\phi$ which is defined by the difference of the work function in vacuum and in the presence of water. Furthermore, we determine the vacuum binding energies of H_2O and *OH species as good descriptors for the prediction of water coverage and thereby

of $\Delta\phi$. Our insights unify different facet geometries and mixed metal surfaces and thereby generalize recent observations. We further present a scheme to predict U_{PZC} based only on the *OH binding and the vacuum work function estimated from static DFT calculations. This formalism is applicable to all investigated metals and mixed metal surfaces including terrace and step geometries and does not require expensive AIMD simulations. To evaluate physical influences to U_{PZC}, we decompose $\Delta\phi$ into its orientational ($\Delta\phi_{\mathrm{orient}}$) and electronic ($\Delta\phi_{\mathrm{el}}$) component. We find $\Delta\phi_{\mathrm{orient}}$ to be a facet dependent property and a major contributor to $\Delta\phi$ on (211) surfaces, while $\Delta\phi_{\mathrm{el}}$ strongly depends on the metal identity.

Introduction

We define the potential of zero charge (U_{PZC}) in this work as the potential at which no excess charge exists on a metal electrode in contact with an electrolyte. This property of metal-water interfaces is an important parameter determining electrochemical behavior [1, 2]. For example, the U_{PZC} determines the strength of the electric field at the interface at an applied potential, and hence the structure of the electric double layer (EDL).[3, 4] The structure of the EDL is in turn crucial in determining electrocatalytic activity and in rationalizing electrolyte effects (e.g. the electrolyte pH and cations) for several energy conversion processes occurring at the metal-water interface.[5–7]

Unfortunately, U_{PZC} of a metal-solution interface can be very difficult to measure experimentally. Both the difficulty in handling and preparing pristine single crystal electrodes and the specific adsorption of ions in the potential regions near U_{PZC} interfere with accurate measurements. Due to specific adsorption, U_{PZC} is frequently distinguished as two distinct properties[2]. The potential of zero total charge (U_{PZTC}) is the potential at which the total charge (q) that includes both charging related to adsorption/desorption events (for e.g. H* and OH*) and double layer charging, is equal to zero (q = 0). The potential of zero free charge, according to Trasatti's original definition, (U_{PZFC}), is the potential at which both

q and the free surface charge density (σ) are zero (q = σ = 0), i.e. no specific adsorption at the PZFC. We note, that these definitions have not been consistently used throughout literature, e.g. in recent work the PZC of adsorbate-covered surfaces has been termed PZFC, even though σ includes contributions from excess free charge due to the adsorption [8].

A number of experimental techniques have been employed to estimate U_{PZC} of a metal surface including laser-induced temperature jump experiments,[8–10] capacitive measurements to determine the Gouy-Chapman minimum,[11] and CO displacement measurements.[12] For reactive surfaces such as Pt and Ir,[9, 13] care should be taken in order to decouple the adsorption/desorption of species like *OH and *H in order to estimate U_{PZFC}.

Another way researchers have sought to understand U_{PZC} is through the work function reduction ($\Delta\phi$) which occurs between a surface in water and the same surface in vacuum (ϕ^{vac}). Trasatti showed that U_{PZFC} can be directly derived from the work function of a material in ion-free water ϕ [14]. Because U_{PZC} is measured in V [here vs. the standard hydrogen electrode (SHE)], the following equation can be used to relate ϕ and U_{PZC}:

$$\phi = eU_{PZC} + \phi_{\mathrm{SHE}} \tag{1}$$

ϕ_{SHE} is the absolute potential energy of the SHE. Note that there is uncertainty in the value of ϕ_{SHE} measured from different experiments (4.3-4.8 eV), and the value of 4.44 eV as recommended by the International Union of Pure and Applied Chemistry (IUPAC) will be used in this work.

Using the relation in Equation 1, Trassati attempted to connect U_{PZC} to ϕ^{vac}, as the latter is an easier quantity to measure in experiments [15]. However, these quantities differ significantly, and the difference can be measured using the following equation:

$$\Delta\phi = \phi - \phi^{\mathrm{vac}} = eU_{PZC} + 4.44 - \phi^{\mathrm{vac}} \tag{2}$$

Values for ϕ^{vac}, U_{PZC}, and the work function reduction $\Delta\phi$ for a number of transition

metal surfaces are tabulated in Table S1, where it can be seen that $\Delta\phi$ varies significantly across the surfaces. Because ϕ^{vac} is relatively easy to measure, both via experiments and simulations, understanding trends in $\Delta\phi$ is equivalent to understanding trends in U_{PZC}.

Experimentalists have long studied trends in $\Delta\phi$. In the 1960s, Huber and Kirk measured a steady decrease in the work function of Al as they dosed the surface with sub-monolayer amounts of water [16]. Later, this same study was extended to Fe, Co, Ni, Pt, Au and Cu surfaces [17–21]. In all cases, a reduction in the work function was observed as higher doses of water was added to a surface, before leveling off at some saturation coverage. Furthermore, it was found that the value of this saturation in work function reduction was a surface dependent quantity [17]. These studies offered an indication that $\Delta\phi$ was directly related to both the water coverage and the surface under consideration.

Given the experimental difficulties in measuring U_{PZC} and $\Delta\phi$, *ab initio* methods have been applied to determine these quantities. Such simulations also allow for direct, atomic-scale insight into the structure of the electrode-electrolyte interface. Previous studies have used density functional theory (DFT) simulations with a static layer of water molecules to predict U_{PZC} [22–27], but Schnur et al. showed that these values depend strongly on the initial orientation of the water molecules used in the simulation [22]. Further, methods using implicit solvation models have been shown to have little to no predictive power in U_{PZC} estimations [28]. Consequently, AIMD simulations of metal-water interfaces have emerged as the most accurate method to estimate U_{PZC} ([22, 29–32]). A major issue of this method is its high computational expense relative to static DFT simulations. Thus, it would be beneficial to identify simple descriptors that can be calculated from static DFT simulations to estimate U_{PZC} of a given surface.

Earlier studies have noticed that surfaces having stronger interactions with water also tend to have larger $\Delta\phi$ [22, 29]. In a recent study, Cheng and co-workers [33] found a linear correlation between experimentally measured $\Delta\phi$ and the computed adsorption energy of water on a number of planar [(111), (100), (110) and (0001)] metal surfaces. In addition,

they find a correlation between the computed $\Delta\phi$ and the coverage of chemisorbed water obtained using AIMD simulations.

In this work, we directly correlate $\Delta\phi$ to the coverage of water estimated from AIMD simulations for a large number of bare flat (111, 100 and 0001) and also stepped (211) transition metal-water interfaces. Like in recent work [33], we find the binding energy of H_2O, obtained from static DFT calculations, to be a good descriptor of water coverage and corresponding U_{PZC} on planar surfaces. In addition, we also find OH binding to be a good descriptor, which has a much larger variation across metal surfaces ($>$ 1 eV) than H_2O (ca. 0.3 eV) and also correlates stepped surfaces. It therefore provides a greater accuracy and generality as a descriptor for the prediction of U_{PZC}. We furthermore find these descriptors to also hold for the prediction of the U_{PZC} of overlayer (mixed metal) surfaces. Finally, we evaluate electronic and orientational contributions of $\Delta\phi$. In contrast to previous findings on flat surfaces, we find the latter contribution to be especially relevant for stepped (211) surfaces. While a larger orientational contribution may arise from a different simulation setup, it also highlights the importance of the water geometry in determining the U_{PZC}.

Computational Methods

We used the Vienna Ab Initio Simulation Package (VASP) to perform DFT and AIMD simulations using the revised Perdew-Burke-Ernzerhof (RPBE) [34] exchange correlation (XC) functional with the D3 dispersion correction scheme [35], which has been shown to accurately describe metal-water interfaces [36, 37]. A plane-wave cutoff of 400 eV and a Gaussian smearing of width 0.1 eV were used in our simulations. The electronic structure was relaxed until all forces converged to less than 0.05 eV/Å.

Static DFT and AIMD calculations were carried out on the fcc(111) facet of Ag, Au, Cu, Pd, Pt, and Rh; the fcc(100) and (211) surfaces of Ag, Au, Cu and Pt; and the hcp(0001) surface of Ru. Additionally, systems with one monolayer of either Ag or Pd on the (111)

surface of Pt or Au were considered. 3x4 unit cells were used for fcc(111) and hcp(001) surfaces and 3x3 unit cells were used for the fcc(100) and (211) surfaces. A 4x3x1 Monkhorst k-point grid was used for fcc(111) and hcp(0001) surfaces and (4x4x1) for fcc(100) and (211) surfaces. For the calculations involving pure transition metal surfaces, three vertical layers were used with only the top layer allowed to relax. The monolayer systems consisted of four vertical layers with the top two layers allowed to relax.

Geometry optimizations were relaxed until all forces were below 0.05 eV/Å. Work functions were calculated by subtracting the vacuum potential of the simulation cell from the fermi energy of the same simulation cell. Vacuum electronic binding energies for H_2O and OH were calculated with reference to H_2O and H_2 as:

$$\Delta E_{H_2O} = E_{slab+H_2O} - E_{slab} - E_{H_2O(g)} \tag{3}$$

$$\Delta E_{OH} = E_{slab+OH} - E_{slab} - E_{H_2O(g)} + \frac{1}{2}E_{H_2(g)} \tag{4}$$

To reduce configurational effects on the OH binding energy, the adsorbate was constrained to the ontop site on all flat surfaces and to the step site on (211) surfaces during the geometry optimizations.

AIMD simulations were conducted with a 1 fs timestep employing a Nosé Thermostat set at 300K. The metal-water interfaces for fcc(111) and hcp(0001) surfaces consisted of 24 water molecules, corresponding to roughly three "layers" of static water. The number of water molecules were scaled down by the relative simulation cell size to 21 on the (100) surfaces and 15 on the (211) surfaces (retaining the same water layer thickness). We benchmarked the water layer thickness against simulations with twice the number of water layers for 11 systems including terrace and step surfaces as shown in the supporting information Tab. S3. We find that the average workfunction during the AIMD trajectory (ϕ_{AIMD}) and its polarization and orientation contributions (see below) show almost identical values in agreement with previous work on system size dependence [37]. Cu(111) and Pt(111) are the only exceptions in this

regard as they show larger deviation which we attribute to insufficient statistics, however.

Figure 1a shows a sample snapshot from the AIMD simulations of the Pt(111)-water interface. Four individual AIMD trajectories starting from different initial water configurations were conducted on each investigated metal surface. Such a setup allows for distinct randomization among the trajectories and avoids the possible entrapment in a local minimum of the water structure within the ensemble. Each AIMD trajectory was run for ≈ 50 ps, and all of the data analysis on each trajectory was performed after an equilibration period of 20 ps. The work function was sampled every 0.5 ps, leading to at least 60 samples for each individual trajectory. Figure 1b shows histograms of the work function of the Pt(111)-water interface for the four individual trajectories with fitted normal distributions, including the overall normal distribution. In order to determine the uncertainty in the measured quantities, we report the standard deviation (σ) between the different means of each trajectory (e.g. $\sigma = 0.25$ eV for Pt(111) as shown in 1b). As shown in Figure 1c for the example of Pt(111), our simulation setup also reproduces a physical interface where the water layer includes a "bulk"-phase with the density of liquid water.

The water coverage was calculated by averaging the total number of adsorbed H_2O molecules during an AIMD trajectory ($\langle n_{H_2O} \rangle$), and normalizing this value by the number of surface sites - 12 for fcc(111) and hcp(0001), 9 for fcc(100) and fcc(211). We also introduce a site-specific normalization ($\langle \tilde{n}_{H_2O} \rangle$) for fcc(211) facets where contributions for (211) step and (111) terrace sites are separated. We obtained a (211) step specific $\langle \tilde{n}_{H_2O} \rangle$ per site value by proportionally subtracting the separately calculated (111) specific $\langle n_{H_2O} \rangle$ per site values from the total $\langle n_{H_2O} \rangle$ obtained on the fcc(211) facet as

$$\langle \tilde{n}_{H_2O} \rangle^{211}_{\text{per site}} = (\langle n_{H_2O} \rangle^{211}_{\text{total}}/3) - 2 * \langle n_{H_2O} \rangle^{111}_{\text{per site}} \tag{5}$$

We defined a water molecule as adsorbed if the central O atom of the molecule was closer to the surface than the average distance between the first H_2O bilayer and the top

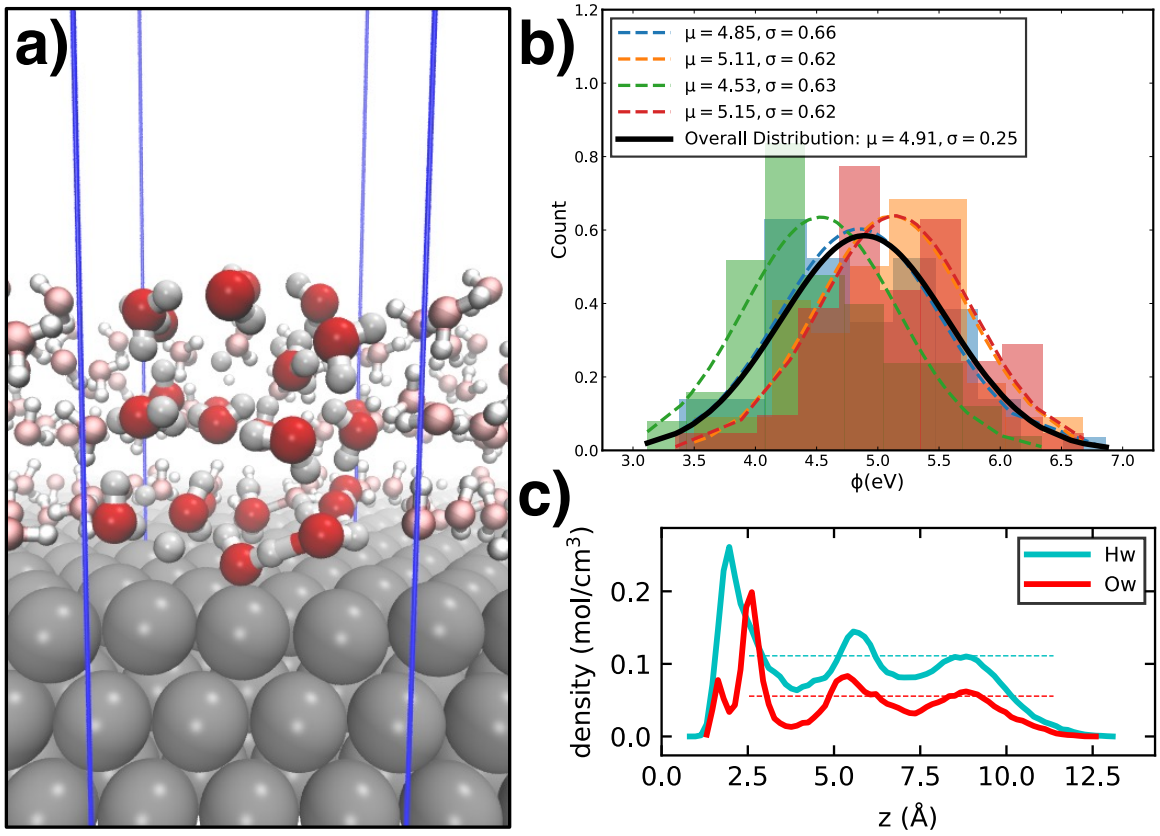

Figure 1: An example of the typical output from an AIMD run showing (a) a snapshot of the Pt(111)-water interface used in the AIMD simulations, (b) histograms of the work functions calculated for the Pt(111)-water interface from four individual runs and the overall normal distribution, and (c) average atomic densities of O (O_w) and H (H_w) from water at the Pt(111)-water interface. For reference, the experimental atomic densities of liquid water are depicted in dashed lines.

metal layer which was determined from a radial distribution function [37]. We found that this characteristic distance $r_{H_2O,Me}$ approximately scales with the covalent radius r_{cov} of the metal. In reference to the Cu specific distance $r_{H_2O,Cu} = 2.55$ Å, estimated from the radial distribution functions of water on Cu(111) and Cu(211) [37], we calculate $r_{H_2O,M}$ as

$$r_{H_2O,Me} = 2.55\text{Å} \cdot \frac{r_{cov,Me} + r_{cov,O}}{r_{cov,Cu} + r_{cov,O}}. \tag{6}$$

In this study we used r_{cov} of a given element as reported in [38].

To investigate the physical nature of $\Delta\phi$ across surfaces, $\Delta\phi$ was decomposed into an

electronic ($\Delta\phi_{\text{el}}$) and an orientational ($\Delta\phi_{\text{orient}}$) contribution, as proposed by Trasatti [14]. Here, $\Delta\phi_{\text{el}}$ is considered to be the potential change due to the electronic redistribution that occurs upon water adsorption on the surface, and $\Delta\phi_{\text{orient}}$ is the potential change due to the orientation of water at the interface.

$$\Delta\phi = \Delta\phi_{\text{el}} + \Delta\phi_{\text{orient}} \tag{7}$$

$\Delta\phi_{\text{el}}$ is calculated using the electron density difference ($\Delta\rho$(z)) along the surface normal z and integrated over x and y. The difference is computed between a snapshot in an AIMD trajectory of the metal-water interface (ρ_{AIMD}(z)) and the electron densities of the separated water molecules ($\rho_{\text{H}_2\text{O}}$(z)) and metal surface ($\rho_{\text{Me}}$(z)). Integrating $\Delta\rho(z)$ along the surface normal yields a dipole moment (cf. Eqn. 8), which is converted to $\Delta\phi_{\text{el}}$, the work function reduction due to electron redistribution, as described in [29].

$$\mu(z) = \int z\Delta\rho(z)dz \tag{8}$$

$\Delta\phi_{\text{orient}}$, the work function reduction due to the net dipole orientation of water molecules, was calculated by isolating the solvent (H_2O) molecules and calculating the outer (Volta) potential difference between the vacuum regions on either side of them [39]. With few exceptions, namely Pt(100), Pt(211), and Pd/Au(111), the calculated values for $\Delta\phi_{\text{el}}$ and $\Delta\phi_{\text{orient}}$ add up to $\Delta\phi$ within 0.1 eV, indicating consistency in accuracy across all 3 values. The higher deviations do not exceed ≤ 0.2 eV which still demonstrates qualitative consistency.

Calculated values for ϕ_{vac}, ϕ_{AIMD}, $\Delta\phi$, $\Delta\phi_{\text{el}}$, $\Delta\phi_{\text{orient}}$, water coverage, $\Delta E_{\text{H}_2\text{O}}$ and ΔE_{OH} are tabulated in Table S2, with standard deviations included for all the averaged quantities obtained from AIMD simulations.

Results and Discussion

Estimated PZCs from AIMD and experiments are consistent, though the agreement arises in part from error cancellation

As detailed in the method section, we use AIMD simulations to predict U_{PZC} on the atomic level for different single crystal facets including fcc(111), fcc(100), fcc(211) and hcp(0001) of a variety of transition metals including Ag, Au, Cu, Pd, Pt, Rh, and Ru. We also considered three overlayer (OL) systems, consisting of metal monolayers on (111) transition metal surfaces: Ag/Au(111), Ag/Pt(111) and Pd/Au(111).

Figure 2 shows a comparison between the computed and experimental values for the work function of the metal surface in vacuum ($\phi^{\mathrm{vac}}_{\mathrm{DFT}}$ and $\phi^{\mathrm{vac}}_{\mathrm{exp}}$), the work function of the metal-water interface (ϕ_{AIMD}) and the potential of zero charge ($U^{\mathrm{PZC}}_{\mathrm{exp}}$), and the work function difference between the metal-water interface and the metal-vacuum interface ($\Delta\phi_{\mathrm{AIMD}}$ and $\Delta\phi_{\mathrm{exp}}$). We see in Figure 2a that $\phi^{\mathrm{vac}}_{\mathrm{DFT}}$ systematically differ from experimental values by about -0.36 eV, which is consistent with previous studies using the RPBE functional without dispersion corrections [40]. As shown in Figure 2c, the computed and experimental values of $\Delta\phi$ show a similar deviation of 0.41 eV, but with the opposite sign. This shift – being constant for all metal substrates – may arise either from the water-vacuum interface, present in all our simulation cells or alternatively by an RPBE functional dependent underprediction of water binding (e.g. in comparison to PBE-D3[22, 29]) which may alter U_{PZC} [33] (see below). The two errors shown in Figures 2a and c cancel out to result in a remarkable consistency between the work function from AIMD (ϕ_{AIMD}) and the experimental $U^{\mathrm{PZC}}_{\mathrm{exp}}$ (Figure 2b), if is ϕ_{AIMD} referenced to the experimental value for the work function of the SHE $\phi_{\mathrm{SHE}} = 4.44$ eV. [41].

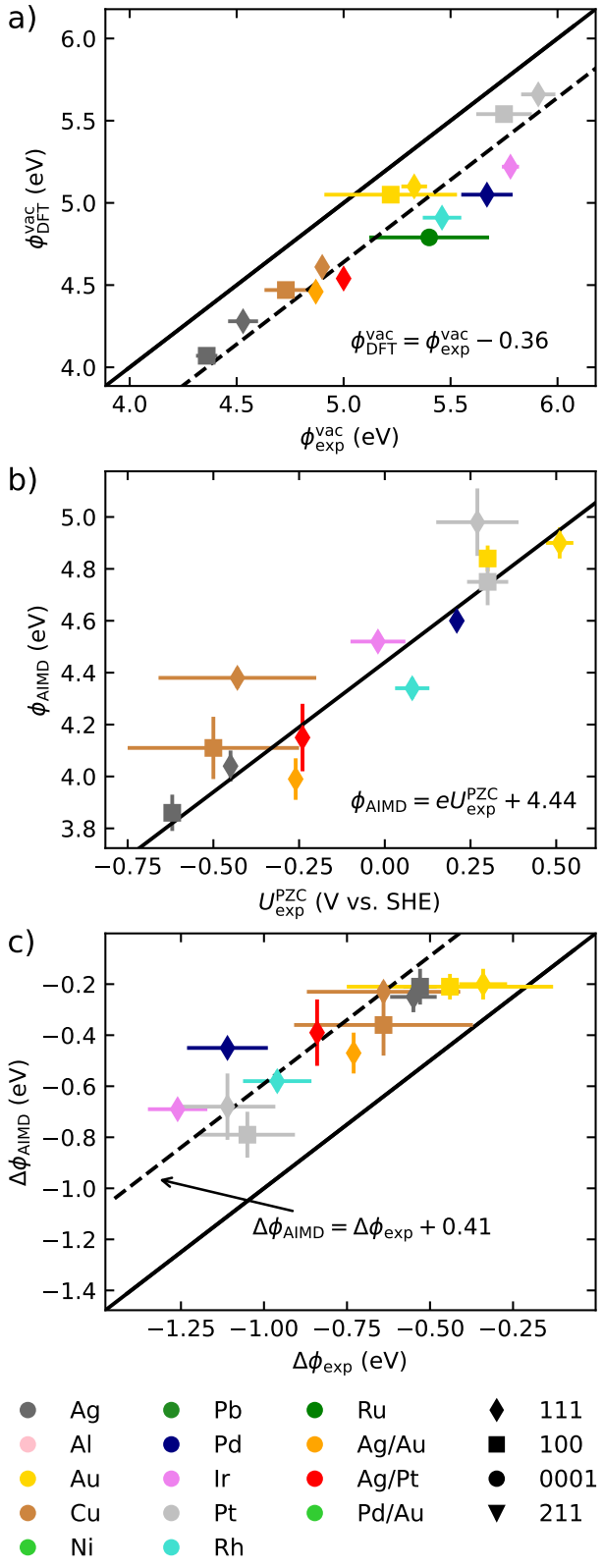

Figure 2: Parity plots between experimental and computational results for (a) vacuum work function, (b) experimental potential of zero charge vs work function in water, and (c) work-function reduction $\Delta\phi$. Solid lines represent parity, while dashed lines represent the equation of best fit constrained to a slope of 1.

Vacuum binding energies of H_2O and OH on TM surfaces as descriptors for water coverage and the corresponding PZCs

Having established that static DFT and AIMD simulations predict trends in ϕ^{vac}, U_{PZC} and $\Delta\phi$ with reasonable accuracy albeit including (accountable) systematic shifts, we discuss descriptors for $\Delta\phi_{\text{AIMD}}$ and the resultant U_{PZC} for the transition metal surfaces considered in this work. Figure 3a shows $\Delta\phi_{\text{AIMD}}$ as a function of water coverage estimated from AIMD simulations. Below a coverage of about 0.10 H_2O per site, we see that water coverage ($\langle n_{H_2O} \rangle$) has very little effect on $\Delta\phi_{\text{comp}}$. For higher values of $\langle n_{H_2O} \rangle$, we see a clear trend of $\Delta\phi_{\text{AIMD}}$ increasing in magnitude as water coverage increases, demonstrating a seemingly linear relationship between water coverage and work function reduction. This trend confirms the hypotheses made in previous studies that increasing water interaction strength results in a larger magnitude of $\Delta\phi$ [22, 29, 33]. Interestingly, the 0.24 eV work function reduction seen on weak-binding surfaces of Ag, Au and Cu is similar to the work function reduction $\Delta\phi$ calculated using an implicit solvent model like VASPsol [42] (see Table S4 in the SI). This convergence in $\Delta\phi$ indicates a constant contribution from the bulk dielectric of liquid water in addition to the specific adsorption of H_2O molecules on the surface. The binding energy threshold (see Figure 3b) of convergence thereby coincides with the condensation energy of H_2O of 0.4 eV [43] below which water interaction is more favorable than specific adsorption. We note that such a convergence is absent in the work by Li *et al.* [33], where deviation may be present due to stronger binding through the PBE-D3 functional and the missing systematic influence of the water-vacuum interface.

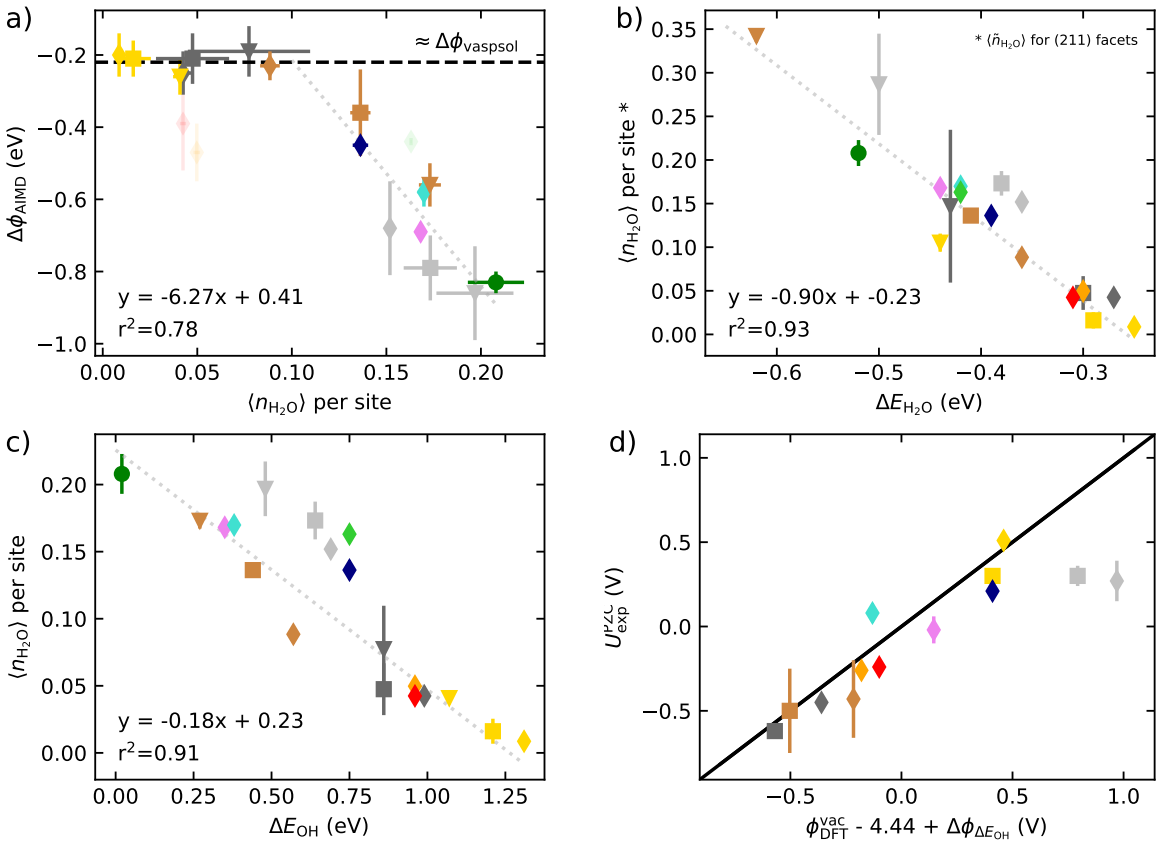

Figure 3: Relationship between a) $\Delta\phi_{\mathrm{AIMD}}$ and water-interaction strength, as described by the adsorption site normalized water coverage $\langle n_{\mathrm{H_2O}}\rangle$ estimated using AIMD simulations, (b) vacuum $\Delta E_{\mathrm{H_2O}}$ and $\langle n_{\mathrm{H_2O}}\rangle$ as well as (c) ΔE_{OH} and $\langle n_{\mathrm{H_2O}}\rangle$. Note that in (b) a corrected site normalized water coverage $\langle\tilde{n}_{\mathrm{H_2O}}\rangle$ was used for (211) facets. (d) Parity plot of predicted U_{PZC} (via equation 10 against available experimentally determined $U_{\mathrm{PZC,exp}}$. Symbols are consistent with Figure 2. Fitted linear correlations (dotted lines) are indicated along with the r^2 values, the fits do not include Pt data points (see text).

The demonstrated correlation of $\langle n_{\mathrm{H_2O}}\rangle$ per site and $\Delta\phi_{\mathrm{AIMD}}$ allows for the prediction of the latter through the estimation of the former. An estimate of $\langle n_{\mathrm{H_2O}}\rangle$ may be evaluated using a simple descriptor that can be obtained from inexpensive static DFT calculations in order to circumvent computationally expensive AIMD simulations. An intuitive choice in this regard would be the electronic binding energy of H_2O in vacuum ($\Delta E_{\mathrm{H_2O}}$) which fulfills this requirement as shown in Figure 3b. This descriptor has also been suggested by Li *et al.* [33] as it works straight-forwardly for terrace sites. For the prediction of (211) step sites, a refined normalization $\langle\tilde{n}_{\mathrm{H_2O}}\rangle$ is required where we distinguish between

contained terrace and step site contributions (see methods Equation 5). This relation using $\langle\tilde{n}_{H_2O}\rangle$ can be useed to reconstruct $\langle n_{H_2O}\rangle$ and thereby unify the prediction for terrace and stepped surfaces. In addition to ΔE_{H_2O} we found that the vacuum adsorption energy of *OH (ΔE_{OH}) also correlates with water adsorption as shown in Figure 3c. Notably, we find it to directly predict the coverage dependent $\langle n_{H_2O}\rangle$ for fcc(211) surfaces. Further, the electronic adsorption energies of ΔE_{OH} span over a wider energy range than ΔE_{H_2O} making it less prone to DFT inaccuracies. From the universal descriptor ΔE_{OH} and its clear correlation with $\langle n_{H_2O}\rangle$, we can deduce a general formula to predict $\Delta\phi_{AIMD}$ through the approximation of $\Delta\phi_{\Delta E_{OH}}$ as

$$\Delta\phi_{\Delta E_{OH}} = min(-0.2, 1.13 \cdot \Delta E_{OH} - 1.03). \tag{9}$$

It follows for the prediction of the $U_{PZC} = \phi^{vac}_{DFT} - 4.44 + \phi_{\Delta E_{OH}}$

$$U_{PZC} = \phi^{vac}_{DFT} - 4.44 + min(-0.2, 1.13 - E_{OH} - 1.03) \tag{10}$$

which correlates well with experimental PZC ($U_{PZC,exp}$ as demonstrated in Figure 3d). We note that this correlation includes the systematic error cancellation of $\phi_{vac,DFT}$ and $\Delta\phi_{AIMD}$ (the latter likely deriving from the water vacuum interface) as discussed above.

We note some noise in the correlations of $\langle\tilde{n}_{H_2O}\rangle$ and $\langle n_{H_2O}\rangle$ with ΔE_{H_2O} and ΔE_{OH}. While some of it may derive from insufficient statistics of the AIMD simulations and of the sampling of adsorption energies, we believe that we also encounter a systematic deviation for all Pt surfaces (Pt(111), Pt(100), and Pt(211)). This deviation becomes most apparent in Figure 3c. It has been previously noted that liquid water is particularly stable on Pt(111) surfaces, a feature which has been attributed to the lattice constant of Pt leading to a relatively unstrained hexagonal ice-like water structure on this surface [44]. It is notable, then, that the Pt(100) and Pt(211) surface also seem to have higher water coverage than ΔE_{OH} would predict, implying that the stability of water on Pt might have a different origin. The outlying Pt data has not been included in the indicated fits in Figure 3. The noted

correlations follow, otherwise, closely a linear trend. It should be noted, however, that these trends do include some error cancellation as the direct correlation between the computed ΔE_{H_2O} or ΔE_{OH} and $\Delta\phi_{AIMD}$ exhibits more noise (see Figure S1).

The three investigated OL systems follow the trends and ΔE_{OH} prediction scheme equally well as the pure metal surfaces as shown in Figure 3b-d, which indicates that the general correlations hold for mixed metal systems. The only deviation between OL and the pure metal systems we observe is in the correlation between the AIMD predicted $\Delta\phi_{AIMD}$ and $\langle n_{H_2O}\rangle$ for the Ag monolayer systems (see Figure 3a). This deviation may be related to the observation that ϕ_{AIMD} appears similar to that of the pure Ag system, despite the higher work function of the overlayer systems in vacuum (see SI Table S2). However, we note that the values for $\Delta\phi_{AIMD}$ could still lie within the error margins of ϕ_{AIMD} (see Figure 2) and future studies considering other OL systems are needed to make definitive conclusions in this regard.

$\Delta\phi_{AIMD}$ arises from both $\Delta\phi_{el}$ and $\Delta\phi_{orient}$; $\Delta\phi_{orient}$ is the major contributor on (211) surfaces

To investigate the origin of $\Delta\phi_{AIMD}$, we performed a decomposition analysis by estimating the electronic and orientational contributions to the $\Delta\phi_{AIMD}$ as discussed in the Methods Section. Figure 4 shows the individual contributions of $\Delta\phi_{orient}$ and $\Delta\phi_{el}$ together with $\Delta\phi_{AIMD}$ for all the TM surfaces considered in this study. In agreement with previous studies, [29, 33] we find $\Delta\phi_{el}$ to be generally larger in magnitude for stronger binding surfaces (Pt, Pd, Ir, Rh, and Ru) and smaller in magnitude for weaker binding surfaces (Cu, Au, and Ag). Previous studies employing AIMD simulations show some disagreement on the magnitude of $\Delta\phi_{orient}$ on flat surfaces, with some finding little to no orientational contribution to $\Delta\phi$ [29, 33], and others reporting larger $\Delta\phi_{orient}$ values (ca. 0.3 to 0.7 eV) on Pt(111) [32, 39]. The $\Delta\phi_{orient}$ estimations in this work generally fall between these values, with $\Delta\phi_{orient} \approx$ 0.4 eV on Pt(111), and ranging between 0-0.4 eV on flat surfaces (i.e. 111, 100 and 0001).

$\Delta\phi_{\text{orient}}$ always screens the influence of $\Delta\phi_{\text{el}}$ by forming a compensating dipole of opposite sign, consistent with the physical picture of the electric double layer. Interestingly, as can be seen in the bottom panel in Figure 4, we find a much larger contribution of $\Delta\phi_{\text{orient}}$ to $\Delta\phi_{\text{AIMD}}$ for the stepped (211) surfaces, with values ranging from 0.8 to 1.2 eV, indicating that $\Delta\phi_{\text{orient}}$ is more of a facet dependent than a metal identity dependent property. Here, the geometry of the pronounced (211) step surface, already forms a surface dipole, which intensifies the orientational contribution. A higher $\Delta\phi_{\text{orient}}$ in stepped surfaces fits the trends reported for (110) vs. (111), (100) surfaces in Refs [29, 33]. However, reported $\Delta\phi_{\text{orient}}$ in these studies have overall a negligible contribution which may be related to the simulation setup employed. According simulation cells consists of a metal-water-metal system instead of a metal-water-vacuum system used in this work.

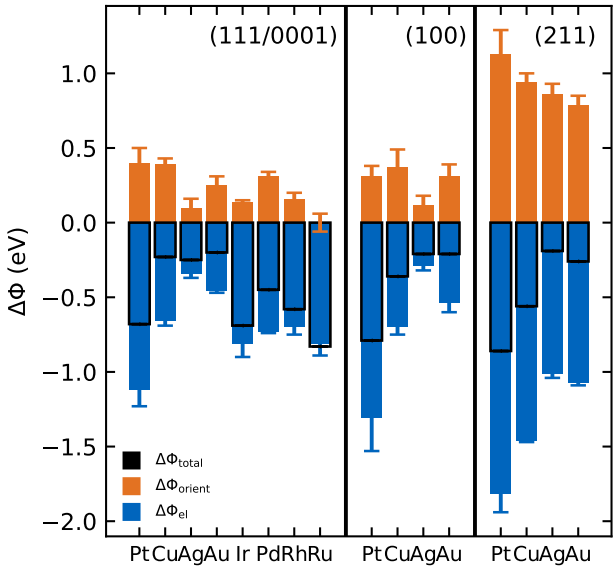

Figure 4: A bar plot showing the individual contributions of $\Delta\phi_{\text{orient}}$ and $\Delta\phi_{\text{el}}$ to the overall $\Delta\phi_{\text{AIMD}}$ for the (111), (0001), (100), and (211) transition metal surfaces considered in this study.

Conclusions

In this work, we performed AIMD simulations on several transition metal-water interfaces to understand the correlation between the potential of zero change (U_{PZC}) and work function reduction ($\Delta\phi$) with the aim to identify simple descriptors to predict these quantities. We find a good correlation between $\Delta\phi$ and the water coverage ($\langle n_{\mathrm{H_2O}} \rangle$) estimated from AIMD simulations of the metal-water interface. Importantly, we also find the vacuum binding energies of H_2O and *OH computed through inexpensive static DFT simulations to exhibit good correlations with $\langle n_{\mathrm{H_2O}} \rangle$. Based on these results, we present a scheme to predict U_{PZC} based only on the *OH binding and the vacuum work function estimated from static DFT calculations, without the need for expensive AIMD simulations. We note, however, that some of these predictions fail, specifically for Pt surfaces, indicating that future work on understanding the relationship between binding energy and coverage of water on Pt is needed. While some of these trends have also recently been demonstrated on flat surfaces by Li *et al.* [33], we extend these insights for stepped fcc(211) and mixed metal overlayer (OL) surfaces and find the correlations between the water coverage and work function reduction to be universal. Finally, we perform a decomposition analysis of the computed reduction in work function into an electronic and orientational components and find that latter is significantly higher for the fcc(211) surfaces compared to the flat (111, 100, 0001) surfaces.

While our AIMD simulations reproduce experimental $\Delta\phi$ and U_{PZC} with a reasonable accuracy, we note that, for many surfaces other than the ones considered here, the available experimental data for U_{PZC} is sparse or non-existent. Because of the importance of U_{PZC} in understanding the structure and properties of electrified metal-water interfaces that are central to several technologically important energy conversion schemes, we implore researchers to continue to pursue experimental methods for the accurate estimation of U_{PZC}. In the meantime, the simple scheme presented in this work based on detailed atomistic simulations of metal-water interfaces can help us understand and predict U_{PZC}, $\Delta\phi$, and its individual contributions.

Code & Data availability

The AIMD trajectories are available through Zenodo with DOI 10.5281/zenodo.5720009. The code used for post processing for all discussed quantities discussed is available under the MIT License on GitHub under .

Acknowledgements

This work was supported by the U.S. Department of Energy, Office of Science, and Office of Basic Energy Science via Grant DE-SC0008685 to the SUNCAT Center of Interface Science and Catalysis. We also acknowledge funding by research grants 9455 and 29450 from VILLUM FONDEN.

References

(1) Schmickler, W. *Chemical Reviews* **1996**, DOI: 10.1021/cr940408c.

(2) Trasatti, S.; Lust, E. In *Modern Aspects of Electrochemistry*, 1999; Chapter 1, pp 1–215.

(3) Le, J.-B.; Cheng, J. *Current Opinion in Electrochemistry* **2021**, *27*, 100693.

(4) Le, J.-B.; Fan, Q.-Y.; Li, J.-Q.; Cheng, J. *Science Advances* **2020**, *6*, eabb1219.

(5) Kelly, S. R.; Kirk, C.; Chan, K.; Nørskov, J. K. *The Journal of Physical Chemistry C* **2020**, DOI: 10.1021/acs.jpcc.0c02127.

(6) Ringe, S.; Morales-Guio, C. G.; Chen, L. D.; Fields, M.; Jaramillo, T. F.; Hahn, C.; Chan, K. *Nature Communications* **2020**, DOI: 10.1038/s41467-019-13777-z.

(7) Ringe, S.; Clark, E. L.; Resasco, J.; Walton, A.; Seger, B.; Bell, A. T.; Chan, K. *Energy and Environmental Science* **2019**, DOI: 10.1039/c9ee01341e.

(8) Auer, A.; Ding, X.; Bandarenka, A. S.; Kunze-Liebhäuser, J. *Journal of Physical Chemistry C* **2021**, *125*, 5028.

(9) Ganassin, A.; Sebastian, P.; Climent, V.; Schuhmann, W.; Bandarenka, A. S.; Feliu, J. *Scientific Reports* **2017**, DOI: 10.1038/s41598-017-01295-1.

(10) Sebastian-Pascual, P.; Sarabia, F. J.; Climent, V.; Feliu, J. M.; Escudero-Escribano, M. *The Journal of Physical Chemistry C* **2020**, DOI: 10.1021/acs.jpcc.0c07821.

(11) Ojha, K.; Arulmozhi, N.; Aranzales, D.; Koper, M. T. *Angewandte Chemie - International Edition* **2020**, *59*, 711–715.

(12) Koga, O.; Matsuo, T.; Hoshi, N.; Hori, Y. *Electrochimica Acta* **1998**, *44*, 903–907.

(13) Sarabia, F. J.; Sebastián-Pascual, P.; Koper, M. T.; Climent, V.; Feliu, J. M. *ACS Applied Materials & Interfaces* **2019**, *11*, 613–623.

(14) Trasatti, S. *Electrochimica Acta* **1991**, *36*, 1659–1667.

(15) Derry, G. N.; Kern, M. E.; Worth, E. H. *Journal of Vacuum Science & Technology A: Vacuum, Surfaces, and Films* **2015**, DOI: 10.1116/1.4934685.

(16) Huber, E. E.; Kirk, C. T. *Surface Science* **1966**, DOI: 10.1016/0039-6028(66)90041-0.

(17) Heras, J. M.; Viscido, L. *Applications of Surface Science* **1980**, DOI: 10.1016/0378-5963(80)90133-6.

(18) Heras, J. M.; Albano, E. V. *Applications of Surface Science* **1981**, DOI: 10.1016/0378-5963(81)90081-7.

(19) Heras, J. M.; Albano, E. V. *Applications of Surface Science* **1983**, DOI: 10.1016/0378-5963(83)90034-X.

(20) Heras, J. M.; Estiú, G.; Viscido, L. *Applied Surface Science* **1997**, DOI: 10.1016/S0169-4332(96)00686-1.

(21) Langenbach, E.; Spitzer, A.; Lüth, H. *Surface Science* **1984**, DOI: 10.1016/0039-6028(84)90174-2.

(22) Schnur, S.; Groß, A. *New Journal of Physics* **2009**, *11*, DOI: 10.1088/1367-2630/11/12/125003.

(23) Meng, S.; Wang, E. G.; Gao, S. *Physical Review B - Condensed Matter and Materials Physics* **2004**, DOI: 10.1103/PhysRevB.69.195404.

(24) Huzayyin, A.; Dawson, F. *Journal of Electroanalytical Chemistry* **2015**, DOI: 10.1016/j.jelechem.2015.04.014.

(25) Filhol, J. S.; Bocquet, M. L. *Chemical Physics Letters* **2007**, *438*, 203–207.

(26) McBride, F.; Omer, A.; Clay, C. M.; Cummings, L.; Darling, G. R.; Hodgson, A. *Journal of Physics Condensed Matter* **2012**, DOI: 10.1088/0953-8984/24/12/124102.

(27) Meng, S.; Wang, E. G.; Frischkorn, C.; Wolf, M.; Gao, S. *Chemical Physics Letters* **2005**, DOI: 10.1016/j.cplett.2004.12.065.

(28) Hörmann, N. G.; Andreussi, O.; Marzari, N. *Journal of Chemical Physics* **2019**, *150*, 41730.

(29) Le, J.; Iannuzzi, M.; Cuesta, A.; Cheng, J. *Physical Review Letters* **2017**, *119*, 1–6.

(30) Duan, S.; Xu, X.; Tian, Z. Q.; Luo, Y. *Physical Review B - Condensed Matter and Materials Physics* **2012**, DOI: 10.1103/PhysRevB.86.045450.

(31) Pedroza, L. S.; Poissier, A.; Fernández-Serra, M. V. *Journal of Chemical Physics* **2015**, DOI: 10.1063/1.4905493.

(32) Sakong, S.; Groß, A. *Journal of Chemical Physics* **2018**, *149*, 084705.

(33) Li, X.-Y.; Chen, A.; Yang, X.-H.; Zhu, J.-X.; Le, J.-B.; Cheng, J. *The Journal of Physical Chemistry Letters* **0000**, *0*, PMID: 34319117, 7299–7304.

(34) Hammer, B.; Hansen, L. B.; Nørskov, J. K. *Phys. Rev. B* **1999**, *59*, 7413.

(35) Grimme, S.; Antony, J.; Ehrlich, S.; Krieg, H. *J. Chem. Phys.* **2010**, *132*, 154104.

(36) Sakong, S.; Forster-Tonigold, K.; Groß, A. *J. Chem. Phys* **2016**, *144*, 194701.

(37) Heenen, H. H.; Gauthier, J. A.; Kristoffersen, H. H.; Ludwig, T.; Chan, K. *Journal of Chemical Physics* **2020**, DOI: 10.1063/1.5144912.

(38) Cordero, B.; Gómez, V.; Platero-Prats, A. E.; Revés, M.; Echeverría, J.; Cremades, E.; Barragán, F.; Alvarez, S. *Journal of the Chemical Society. Dalton Transactions* **2008**, DOI: 10.1039/b801115j.

(39) Bramley, G.; Nguyen, M.-T.; Glezakou, V.-A.; Rousseau, R.; Skylaris, C.-K. *Cite This: J. Chem. Theory Comput* **2020**, *16*, DOI: 10.1021/acs.jctc.0c00034.

(40) Hammer, B.; Hansen, L. B.; Nørskov, J. K. *Physical Review B - Condensed Matter and Materials Physics* **1999**, DOI: 10.1103/PhysRevB.59.7413.

(41) Trasatti, S. *Trends in Interfacial Electrochemistry* **1986**, 25–48.

(42) Mathew, K.; Kolluru, V. C.; Mula, S.; Steinmann, S. N.; Hennig, R. G. *J. Chem. Phys.* **2019**, *151*, 234101.

(43) Wagman, D. D.; Evans, W. H.; Parker, V. B.; Schumm, R. H.; Halow, I.; Bailey, S. M.; Churney, K. L.; Nuttall, R. L. *J. Phys. Chem. Ref. Data* **1982**, *11*.

(44) Tripkovic, V.; Björketun, M. E.; Skúlason, E.; Rossmeisl, J. *PHYSICAL REVIEW B* **2011**, *84*, 115452.

Graphical TOC Entry